Transverse momentum dependent parton distributions of pion at leading twist

Wei Kou,[1,2] Chao Shi,[3,*] Xurong Chen,[1,2,†] and Wenbao Jia[3]

[1]Institute of Modern Physics, Chinese Academy of Sciences, Lanzhou 730000, China
[2]University of Chinese Academy of Sciences, Beijing 100049, China
[3]Department of Nuclear Science and Technology, Nanjing University of Aeronautics and Astronautics, Nanjing 210016, China

(Received 25 April 2023; accepted 10 August 2023; published 29 August 2023)

We calculate the leading twist pion unpolarized transverse momentum distribution $f_1(x, k_T^2)$ and the Boer-Mulders function $h_1^\perp(x, k_T^2)$, using leading Fock-state light front wave functions (LF-LFWFs) based on Dyson-Schwinger and Bethe-Salpeter equations (DS-BSEs). These DS-BSEs based LF-LFWFs provide dynamically generated s- and p-wave components, which are indispensable in producing the chirally odd Boer-Mulders function that has one parton spin flipped. Employing a nonperturbative SU(3) gluon rescattering kernel to treat the gauge link of the Boer-Mulders function, we thus obtain both transverse momentum dependent parton distribution functions at hadronic scale and then evolve them to the scale of $\mu^2 = 4.0\ \mathrm{GeV}^2$. We finally calculate the generalized Boer-Mulders shift and find it to be in agreement with the lattice quantum chromodynamics prediction.

DOI: 10.1103/PhysRevD.108.036021

I. INTRODUCTION

Multidimensional imaging of hadrons has excited a lot of interest for the last several decades. Transverse momentum dependent (TMD) parton distributions functions (PDFs) contain important information of the three-dimensional internal structure of hadrons, especially the spin-orbit correlations of quarks within them [1–5]. The TMD-PDFs of the pion and nucleon, which are spin 0 and spin 1/2, respectively, have thus received extensive studies from phenomenological models [6–11] and lattice QCD [12–15]. Experimentally, they can be studied with the Drell-Yan (DY) or semi-inclusive deep-inelastic scattering (SIDIS) process for nucleons [16–23].

The Boer-Mulders function is a time-reversal odd (T-odd) distribution, which was initially considered to vanish due to the time-reversal invariance of QCD [24], but later it became clear that they could appear dynamically by the initial or final states interaction [25,26]. In other words, the T-odd distribution does not vanish in the case of nontrivial gauge link, which is required by the field theory of color gauge invariance [27–29]. In addition, the gauge link makes the T-odd distribution process dependent and selects the opposite sign depending on the process from SIDIS to DY.

Experimental measurements of the unpolarized pion-induced DY scattering [9,17] cross section and the azimuthal asymmetries are based on the unpolarized TMD-PDF and the Boer-Mulders function of pion as inputs, which had both been measured [30–32]. The azimuthal asymmetry has been observed experimentally, and the pion Boer-Mulders function is important for explaining these observations. In addition to this, little is known about experiments with meson TMD-PDFs, although this may change with the new COMPASS Collaboration program for meson-induced DY scattering [33,34].

Theoretical calculation on the Boer-Mulders function has also received much attention. The pion Boer-Mulders function has been predicted in the antiquark spectator model [35,36], the light front constituent quark model [9,17,37,38], the MIT bag model [39], the Nambu–Jona-Lasinio (NJL) model [10,40], and the light front holographic approach [41]. Except for the approach discussed in Ref. [41], the other previous models consider the interpretation of the Boer-Mulders function by gluon rescattering under perturbative cases. In Ref. [42], the authors have made a notable attempt to go beyond this perturbative approximation within the antiquark spectator framework. Meanwhile, lattice calculation related to the pion Boer-Mulders function can also be found in the literature [12,43].

Here we take the light front QCD framework, where the TMD-PDFs are determined through overlap representations

*cshi@nuaa.edu.cn
†xchen@impcas.ac.cn

in terms of light front wave functions [44,45]. In [11], we employed the Dyson-Schwinger and Bethe-Salpeter equations (DS-BSEs) based leading Fock-state light front wave functions (LF-LFWFs) and calculate the unpolarized TMD-PDF of pion in the chiral limit. Here we will employ the LF-LFWFs of pion at physical mass from [46] and calculate the two leading-twist TMD-PDFs for pion. Our focus here is the Boer-Mulders function. According to the overlap representation at leading Fock-state, the Boer-Mulders function is proportional to p-wave ($q\bar{q}$ spin parallel) components of the LF-LFWFs [41]. Hence it provides a sensitive probe to the p-wave components inside pion. In the light cone constituent quark model, all spin configurations are generated by the Melosh rotation [47]. A modeling scalar function is then introduced to count in the dynamical effect [9,48]. In the light front holographic approach, as the conventional holographic pion LFWF only has spin-anti-parallel contribution [49,50], the authors add spin-parallel terms that are modulated by a dynamical spin parameter B, with B phenomenologically determined from pion decay constant and form factors [41,51]. Here in the DS-BSEs approach, the s- and p-wave LFWF components are simultaneously determined from their parent Bethe-Salpeter wave function, which are dynamically solved, so the ratio between them is fixed [46]. Given the Boer-Mulders function's sensitivity to p-wave components, it is thus worth investigating the prediction from DS-BSEs based LF-LFWFs on the pion Boer-Mulders function.

This paper is organized as follows: In Sec. II, we recapitulate the LF-LFWFs of pion from its Bethe-Salpeter wave functions. We then introduce the pion unpolarized TMD-PDF and Boer-Mulders function in Sec. III. The rescattering kernel of the SU(3) non-Abelian gluon is employed and used to compute the gauge link in the Boer-Mulders function. The evolution of pion TMD-PDFs and comparison to lattice QCD regarding the generalized Boer-Mulders shift [12] are represented in Sec. IV. Finally, we conclude in Sec. V.

II. PION LIGHT FRONT WAVE FUNCTIONS

In light front QCD hadron states can be expressed as the superposition of Fock-state components classified by their orbital angular momentum projection l_z [29]. For a pion with valence quark f and valence antiquark $\bar{h}$ that has zero transverse momentum, the minimal (two-particle) Fock-state configuration is given by [52,53]

$$|M\rangle = \sum_{\lambda_1,\lambda_2} \int \frac{d^2\mathbf{k_T}}{(2\pi)^3} \frac{dx}{2\sqrt{x\bar{x}}} \frac{\delta_{ij}}{\sqrt{3}} \times \Psi_{\lambda_1,\lambda_2}(x,\mathbf{k_T}) b^\dagger_{f,\lambda_1,i}(x,\mathbf{k_T}) d^\dagger_{\bar{h},\lambda_2,j}(\bar{x},\bar{\mathbf{k}}_\mathbf{T})|0\rangle, \quad (1)$$

where $\mathbf{k_T} = (k^x, k^y)$ is the transverse momentum of the quark f, $\bar{\mathbf{k}}_\mathbf{T} = -\mathbf{k_T}$, $x = \frac{k^+}{P^+}$ is the light cone momentum fraction of the active quark, and $\bar{x} = (1-x)$. The light front four-vector components take the notation $A^\pm = (A^0 \pm A^3)/2$ throughout this paper. The quark helicity is labeled by $\lambda_i = (\uparrow, \downarrow)$ and $\delta_{ij}/\sqrt{3}$ is the color factor. The $b^\dagger$ and $d^\dagger$ are the creation operators for a quark and antiquark, respectively. The $\Psi_{\lambda_1,\lambda_2}$ are the LF-LFWFs of the pion that encode the nonperturbative internal dynamical information. Meanwhile, constrained by parity properties, the four $\Psi_{\lambda_1,\lambda_2}$'s can be expressed with two independent scalar amplitudes [54],

$$\begin{aligned} \Psi_{\uparrow,\downarrow}(x,\mathbf{k_T}) &= \psi_0(x,\mathbf{k_T}^2), \qquad \Psi_{\downarrow,\uparrow}(x,\mathbf{k_T}) = -\psi_0(x,\mathbf{k_T}^2), \\ \Psi_{\uparrow,\uparrow}(x,\mathbf{k_T}) &= k_T^{(-)}\psi_1(x,\mathbf{k_T}^2), \qquad \Psi_{\downarrow,\downarrow}(x,\mathbf{k_T}) = k_T^{(+)}\psi_1(x,\mathbf{k_T}^2), \end{aligned} \quad (2)$$

where $k_T^{(\pm)} = k^1 \pm ik^2$. The subscript i in ψ_i refers to the absolute value of orbital angular momentum between quark and antiquark projected onto the longitudinal direction. Note that, in the light front constituent quark model and modified holographic model [9,41], the $\psi_0(x,\mathbf{k_T}^2)$ and $\psi_1(x,\mathbf{k_T}^2)$ assumed the same functional form, which does not necessarily hold in a general case [54,55]. In the DS-BSEs approach, they are obtained from the Bethe-Salpeter wave function $\chi(k,P)$ via the light front projections [11,56,57],

$$\psi_0(x,\mathbf{k_T}^2) = \sqrt{3}i \int \frac{dk^+dk^-}{2\pi} \mathrm{Tr}_D[\gamma^+\gamma_5\chi(k,P)]\delta(xP^+ - k^+), \quad (3)$$

$$\psi_1(x,\mathbf{k}_\mathbf{T}^2) = -\sqrt{3}i \int \frac{dk^+dk^-}{2\pi} \frac{1}{\mathbf{k_T}^2} \mathrm{Tr}_D[i\sigma^{+i}k_{Ti}\gamma_5\chi(k,P)]\delta(xP^+ - k^+), \quad (4)$$

where $\sigma^{+i} = \frac{i}{2}[\gamma^+,\gamma^i]$ and the trace is over Dirac indices. The momentum of the quark is $k^\mu = (k^+,k^-,\mathbf{k_T})$ and $P^\mu = (P^+,P^-,\mathbf{0})$ is the meson's momentum. The integrations of $k^\pm$ both run from negative infinity to positive infinity.

The $\chi(k,P)$ can be solved by aligning the quark propagator's Dyson-Schwinger equation and meson Bethe-Salpeter equation [58], i.e.,

$$S(k)^{-1} = Z_2 i\gamma\cdot k + Z_4 m(\mu) + Z_1 \int_q^\Lambda g^2 D_{\mu\nu}(k-q)\frac{\lambda^a}{2}\gamma_\mu S(q)\Gamma^a_\nu(q,k), \quad (5)$$

$$\Gamma(k;P) = \int_q^\Lambda K(k,q;P)S(q_+)\Gamma(q,P)S(q_-). \quad (6)$$

Here $\int_q^\Lambda$ refers to $\int_{-\infty}^{\infty}\frac{d^4q}{(2\pi)^4}$ using a Poincaré invariant regularization with regularization scale Λ. The $D_{\mu\nu}$ is the full gluon propagator in the Landau gauge. The Γ^a_ν and $K(k,q;P)$ are the full quark-antiquark-gluon vertex and quark-antiquark interaction kernel, respectively. The quark momentum partition is $q_\pm = q \pm P/2$ and should not be confused with the aforementioned light front components $k^\pm$. The $m(\mu)$ is the current quark mass renormalized at scale of μ. The Z_2 and Z_4 are the quark wave function and mass renormalization constants, respectively. The $S(k)$ and $\Gamma(k,P)$ are the full quark propagator and Bethe-Salpeter amplitude, respectively. The pion Bethe-Salpeter wave function $\chi(k,P)$ can be expressed as $\chi(k,P) = S(k_+)\Gamma(k,P)S(k_-)$.

In solving Eqs. (5) and (6), we take the rainbow-ladder truncation, e.g.,

$$Z_1\int_q^\Lambda g^2 D_{\mu\nu}(k-q)\Gamma^a_\nu(q,k) \to Z_2^2\int_q^\Lambda \mathcal{G}[(k-q)^2]D^{\rm free}_{\mu\nu}(p-q)\frac{\lambda^a}{2}\gamma_\nu, \quad (7)$$

$$K(k,q;P)\to -Z_2^2\mathcal{G}[(k-q)^2]D^{\rm free}_{\mu\nu}(k-q)\left(\frac{\lambda^a}{2}\gamma_\mu\right)\otimes\left(\frac{\lambda^a}{2}\gamma_\nu\right). \quad (8)$$

The modeling function $\mathcal{G}$ in Eqs. (7) and (8) thus absorbs simultaneously the strong coupling constant α_s, as well as the dressing effect in both the quark-gluon vertex and full gluon propagator. Here we take the Qin-Chang model [59]

$$\mathcal{G}(s) = \frac{8\pi^2}{\omega^4}D e^{-s/\omega^2} + \frac{8\pi^2\gamma_m}{\ln[\tau + (1+s/\Lambda^2_{\rm QCD})^2]}\mathcal{F}(s), \quad (9)$$

which is as equally good as the Maris-Tandy model [58] in hadron studies. The parameter setup in this work follows exactly the same as in our previous work [46] and produces a pion of mass 130 MeV. We note that starting with exactly same setup within DS-BSEs, the ρ and J/ψ LF-LFWFs had been extracted and well reproduced the diffractive meson production cross section within the color dipole model [60]. The generalized parton distribution and leading-twist time-reversal even TMD-PDFs were also studied for light and heavy vector mesons [61,62].

III. TRANSVERSE MOMENTUM DEPENDENT PARTON DISTRIBUTIONS

In this section, we unify the momentum and impact parameter-related symbols as follows:

$$|\mathbf{k_T}| = |\mathbf{k}| = k_T, \qquad |\mathbf{q_T}| = |\mathbf{q}| = q_T, \qquad |\mathbf{b_T}| = |\mathbf{b}| = b_T. \quad (10)$$

A. TMD-PDFs with LFWFs

For the pion, there are two twist-2 TMD-PDFs: the unpolarized quark TMD-PDF $f_1(x,k_T)$ and the polarized quark TMD-PDF $h_1^\perp(x,k_T)$, also known as the Boer-Mulders function [2,63]. The pion TMD-PDFs are derived from the quark correlation function [2,16,64]

$$\Phi^{[\Gamma]}_{ij}(x,\mathbf{k}) = \int\frac{dz^- d^2z_T}{2\pi(2\pi)^2}e^{iz\cdot k}\langle\pi|\bar\Psi_j(0)\Gamma\mathcal{L}^\dagger(\mathbf{0}|n)\mathcal{L}(\mathbf{z}|n)\Psi_i(z)|\pi\rangle_{z^+=0}, \quad (11)$$

where the gauge link content is described as [2,16,64]

$$\mathcal{L}_{A^+=0}(\mathbf{z}_T|n) = \mathcal{P}\exp\left(-ig\int_{\mathbf{z}_T}^\infty d\eta_T\cdot\mathbf{A}_T(\eta^- = n\cdot\infty,\mathbf{z}_T)\right), \quad (12)$$

which guarantees color gauge invariance and $n = (0,+1(-1),0)$ are appropriate for defining TMD-PDFs in SIDIS (Drell-Yan) processes. In particular, this reverses the sign of all T-odd distribution functions entering the correlator [9]. The unpolarized TMD-PDF and Boer-Mulders function are given by [9]

$$f_1(x,k_T) = \frac{1}{2}\mathrm{Tr}\left(\Phi^{[\gamma^+]}\right), \quad (13)$$

and

$$h_1^\perp(x,k_T) = \frac{\epsilon^{ij}\mathbf{k}^j M_\pi}{2k_T^2}\mathrm{Tr}\left(\Phi^{[i\sigma^{i+}\gamma_5]}\right), \quad (14)$$

respectively.

Without consideration of the gauge link, the trace of the quark correlation is written as [41]

$$\mathrm{Tr}(\Phi^{[\Gamma]}) = \sum_{h,\bar h,h'}\frac{1}{16\pi^3 k^+}\Psi^*_{h'\bar h}(x,\mathbf{k})\Psi_{h\bar h}(x,\mathbf{k}) \times\bar u_{h'}(k^+,\mathbf{k})\Gamma u_h(k^+,\mathbf{k}). \quad (15)$$

For unpolarized the TMD-PDF $f_1(x,k_T)$, one has $\Gamma=\gamma^+$ and the light front matrix element [65] is

$$\bar{u}_{h'}(k^+,\mathbf{k})\gamma^+u_h(k^+,\mathbf{k})=2k^+\delta_{hh'}. \tag{16}$$

From Eq. (13) one has

$$f_1(x,k_T)=\frac{1}{16\pi^3}\sum_{h,\bar{h}}|\Psi_{h\bar{h}}(x,\mathbf{k})|^2. \tag{17}$$

In a parton model, integrating over $\mathbf{k}$ in $f_1(x,k_T)$ gives the familiar collinear valence parton distribution $f_1(x)$ [66].

On the other hand, for the Boer-Mulders function (14), the light front matrix element is

$$\bar{u}_{h'}(k^+,\mathbf{k})i\epsilon^{ij}k^j\sigma^{i+}\gamma^5u_h(k^+,\mathbf{k})=2ik^+h'\delta_{-h'h}k_Te^{-ih'\theta_{k_T}}. \tag{18}$$

Substituting Eqs. (1), (2), and (18) into Eq. (15) one gets a vanishing Boer-Mulders function because

$$\sum_{h,\bar{h}}\Psi^*_{-h\bar{h}}(x,\mathbf{k})hk_Te^{ih\theta_{k_T}}\Psi_{h\bar{h}}(x,\mathbf{k})=0. \tag{19}$$

In this case, the gauge link must be taken into consideration. Dynamically, T-odd PDFs emerge from the gauge link structure of the multiparton quark and/or gluon correlation functions [25,27,29,67] which describe initial- and final-state interactions (FSIs) of the active parton via soft gluon exchanges with the target remnant [42]. Many studies have been performed to model the T-odd PDFs in terms of the FSIs where soft gluon rescattering is approximated by perturbative one-gluon exchange in Abelian models [8,25,28,68–74]. In Ref. [42], the authors go beyond this approximation by applying nonperturbative eikonal methods to calculate higher-order gluonic contributions from the gauge link, while also taking into account color, which is collectively referred to as gluon rescattering. In [41], the authors assumed the physics to be encoded in a gluon rescattering kernel $G(x,\mathbf{k}-\mathbf{k}')$ such that

$$\mathrm{Tr}(\Phi^{[\Gamma]})=\sum_{h,\bar{h},h'}\int\frac{\mathrm{d}^2\mathbf{k}'}{16\pi^3k'^+}G(x,\mathbf{k}-\mathbf{k}')\Psi^*_{h'\bar{h}}(x,\mathbf{k}')\times\Psi_{h\bar{h}}(x,\mathbf{k})\bar{u}_{h'}(k'^+,\mathbf{k}')\Gamma u_h(k^+,\mathbf{k}). \tag{20}$$

Inserting Eq. (18) into (20), Eq. (14) yields

$$h_1^\perp(x,k_T^2)=\frac{M_\pi}{k_T^2}\int\frac{\mathrm{d}^2\mathbf{k}'}{16\pi^3}iG(x,\mathbf{k}-\mathbf{k}')\times\sum_{h,\bar{h}}\Psi^*_{-h,\bar{h}}(x,\mathbf{k}')hk_Te^{ih\theta_{k_T}}\Psi_{h,\bar{h}}(x,\mathbf{k}). \tag{21}$$

Determining the $G(x,\mathbf{k}-\mathbf{k}')$ thus would allow us to extract the Boer-Mulders function.

B. Lensing function and gluon rescattering kernel

An exact nonperturbative computation of a gluon rescattering kernel is yet not available and, in practice, some approximation scheme is necessary. Here we take the idea of the chromodynamic lensing function introduced in [75]. It had been applied to the study of phenomenology of the Sivers asymmetry [76] and discussions on its validity and limitations in model studies had been given in [77]. The authors of Ref. [42] show that one could apply nonperturbative eikonal methods to calculate higher-order gluonic contributions from the gauge link to obtain the QCD lensing function [78] from the eikonal amplitude for quark-antiquark scattering via the exchange of both direct and crossed ladder diagrams of non-Abelian soft gluons. According to the scheme of Ref. [42], the lensing function in momentum space $I(x,q_T)$ connects the first moment of the Boer-Mulders function with the chiral-odd pion generalized parton distribution (GPD) [36],

$$M_\pi^2h_1^{\perp(1)}(x)=\int\frac{\mathrm{d}^2\mathbf{q}}{2(2\pi)^2}q_TI(x,q_T)\mathcal{H}_1^\pi\left(x,-\left(\frac{q_T}{\bar{x}}\right)^2\right), \tag{22}$$

where the chiral-odd pion GPD is given by [36]

$$\mathcal{H}_1^\pi(x,-\Delta_T^2)=\frac{\epsilon^{ij}\Delta^iM_\pi}{2\Delta_T^2}\int\frac{\mathrm{d}z^-}{2\pi}e^{ik^+z^-}\langle P^+,\mathbf{\Delta}|\bar{\Psi}(0)\sigma^{i+}\gamma_5\Psi(z)|P^+,\mathbf{0}\rangle_{z^+=0}, \tag{23}$$

with $\mathbf{\Delta}=-\mathbf{q}/\bar{x}$ and $\mathbf{q}=\mathbf{k}-\mathbf{k}'$ denoting the momentum transfer. As noted in Ref. [42], the factorization (22) does not hold, in general [36,79]. However, in Ref. [41] the authors have shown that the factorization also holds in the overlap representation with modified holographic LFWFs. Here we find it holds for our DS-BSEs based LFWFs as well. The lensing function and the gluon rescattering kernel are thus connected as [41]

$$iG(x,q_T)=-\frac{2}{(2\pi)^2}\frac{\bar{x}I(x,q_T)}{q_T}. \tag{24}$$

The lensing function is derived for final-state rescattering by soft U(1), SU(2), and SU(3) gluons. In Ref. [42], the authors derive the eikonal amplitude for quark-antiquark scattering via the exchange of generalized infinite ladders of gluons of the Abelian and non-Abelian case. In all three

cases, the lensing function is negative. In the impact parameter space, the eikonal amplitude yields the lensing function of the form [42]

$$\mathcal{I}(x,b_T)=\frac{\bar{x}}{2N_c}\frac{\chi'}{4}C\left(\frac{\chi}{4}\right), \tag{25}$$

$$C\left[\frac{\chi}{4}\right]\equiv\left[(\mathrm{Tr}\mathfrak{T}[f])'\left(\frac{\chi}{4}\right)+\frac{1}{2}\mathrm{Tr}\left[(\mathfrak{T}[f])'\left(\frac{\chi}{4}\right)(\mathfrak{R}[f])\left(\frac{\chi}{4}\right)\right]-\frac{1}{2}\mathrm{Tr}\left[(\mathfrak{T}[f])\left(\frac{\chi}{4}\right)(\mathfrak{R}[f])'\left(\frac{\chi}{4}\right)\right]\right], \tag{26}$$

where χ' denotes the first derivative with respect to $b_T/\bar{x}$, and $(\mathfrak{T}[f])'$ and $(\mathfrak{R}[f])'$ are the first derivatives of the real and imaginary parts of the color function f. The eikonal phase χ is defined as the Hankel transformation of the gauge-independent part of the gluon propagator $\tilde{\mathcal{D}}_1(-k_T^2)$ [42],

$$\chi\left(\frac{b_T}{\bar{x}}\right)=\frac{g^2}{2\pi}\int_0^\infty dk_T k_T J_0\left(\frac{b_T}{\bar{x}}k_T\right)\mathcal{D}_1(-k_T^2), \tag{27}$$

where J_0 is a Bessel function of the first kind. The coupling g represents the strength of the quark (antiquark)-gluon interaction.

For SU(3) gluons, the real and imaginary parts of the color function f are derived in Ref. [42]. One can get the powerlike forms with the numerical parameters [42]

$$\begin{aligned}\Re[f^{SU(3)}_{\alpha\beta}](a)&=\delta_{\alpha\beta}\left(-c_2a^2+c_4a^4-c_6a^6-c_8a^8+\cdots\right),\\ \Im[f^{SU(3)}_{\alpha\beta}](a)&=\delta_{\alpha\beta}\left(c_1a-c_3a^3+c_5a^5-c_7a^7+\cdots\right),\end{aligned} \tag{28}$$

where $a=\chi/4$ and the parameters' values are set as $c_1=5.333$, $c_2=6.222$, $c_3=3.951$, $c_4=1.934$, $c_5=0.680$, $c_6=0.198$, $c_7=0.047$, and $c_8=0.00967$ [42].

In order to compute the eikonal phase, we follow the previous work [42] and use the nonperturbative Dyson-Schwinger gluon propagator, which has been given in Refs. [80–82],

$$\mathcal{D}_1(k_T^2,\Lambda^2_{\mathrm{QCD}})=\frac{1}{k_T^2}\left(\frac{\alpha_s(k_T^2)}{\alpha_s(\Lambda^2_{\mathrm{QCD}})}\right)^{1+2\delta}\times\left(\frac{c(k_T^2/\Lambda^2)^\kappa+d(k_T^2/\Lambda^2)^{2\kappa}}{1+c(k_T^2/\Lambda^2)^\kappa+d(k_T^2/\Lambda^2)^{2\kappa}}\right)^2, \tag{29}$$

where the running strong coupling α_s presented in [80] is

$$\alpha_s(\mu^2)=\frac{\alpha_s(0)}{\ln\left[\mathrm{e}+a_1(\mu^2/\Lambda^2)^{a_2}+b_1(\mu^2/\Lambda^2)^{b_2}\right]}. \tag{30}$$

The values for the fitting parameters are $\Lambda=0.71$ GeV, $a_1=1.106$, $a_2=2.324$, $b_1=0.004$, and $b_2=3.169$. Note that, in solving the pion Bethe-Salpeter wave functions, we used a different interaction model (9). Therein, the full gluon propagator, the strong coupling constant, and the full quark-gluon vertex are grouped and cannot be separated. So here we employ Eq. (29) instead, which also allows direct comparison with results from [41].

Finally, the momentum space lensing function is given by the inverse Fourier transformation [41],

$$I(x,q_T)\frac{\mathbf{q}^i}{q_T}=-\frac{i}{\bar{x}^3}\int \mathrm{d}^2\mathbf{b}\exp\left(-i\frac{\mathbf{q}\cdot\mathbf{b}}{\bar{x}}\right)\mathcal{I}(x,b_T)\frac{\mathbf{b}^i}{b_T}. \tag{31}$$

From Eqs. (24) to (31), one can calculate the whole lensing function in momentum space $I(x,q_T)$ and eventually the gluon rescattering kernel $iG(x,q_T)$.

C. $f_1(x,k_T)$ and $h_1^\perp(x,k_T)$ at initial scale $\mu=\mu_0$

Having specified both the light front wave functions and the gluon rescattering kernel, we are now in the position to study the pion TMD-PDFs. According to Eqs. (17) and (21), our calculated Boer-Mulders function and unpolarized TMD-PDF are shown in Fig. 1. Note that there is some nonsmoothness in the plots, which is nonphysical and originates in the pion light front wave functions taken

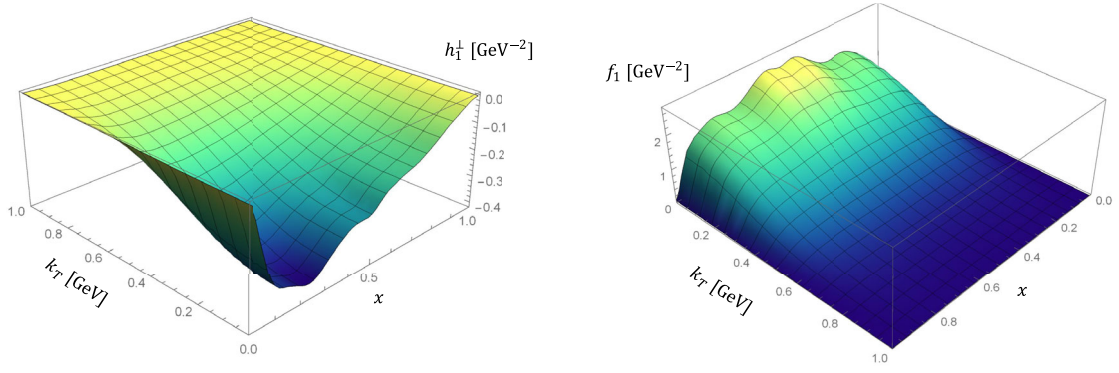

FIG. 1. Left: the Boer-Mulders function generated by the nonperturbative kernel. Right: the unpolarized TMD-PDF f_1.

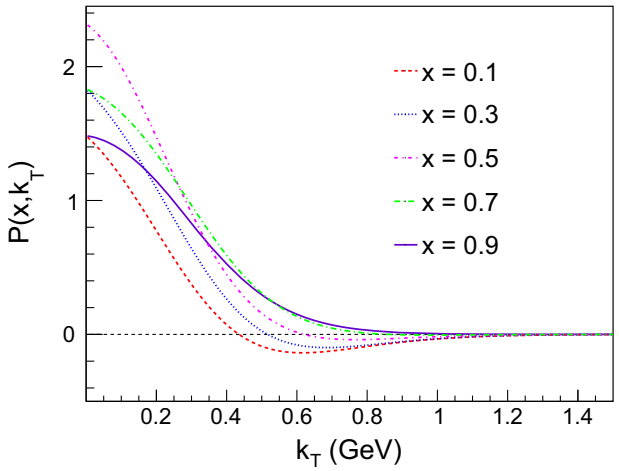

FIG. 2. $P(x, k_T)$ with the Boer-Mulders function generated by the nonperturbative kernel at $x = 0.1$, $x = 0.3$, $x = 0.5$, $x = 0.7$, and $x = 0.9$.

directly from [46]. It is mainly caused by the parametrization procedure therein, which can be improved with a more sophisticated parametrization form or fitting method. Here we stick to those LF-LFWFs and aim for their direct prediction on pion TMD-PDFs.

We first check the general constraint of the positivity bound condition [83] using our TMD-PDFs,

$$P(x, k_T) \equiv f_1(x, k_T) - \frac{k_T}{M_\pi}|h_1^\perp(x, k_T)| \geq 0. \quad (32)$$

In Fig. 2 we show that this constraint is mostly satisfied, with violations only occurring for small x at moderate and large k_T. We note that similar violations were reported in model studies [9,66,84,85] with the perturbative kernel. They indicate a limitation of current nonperturbative models to accurately capture the large k_T behavior of the TMD-PDFs [41]. Theoretically, this issue is supposed to be fixed if both TMD-PDFs are calculated to same order [85]. Fortunately, in our case, the violation is generally small in magnitude and insignificant for $x \gtrsim 0.5$. This is compatible with the leading Fock-state truncation we employ, which works better in the valence region.

IV. THE GENERALIZED BOER-MULDERS SHIFT

Parton distribution functions are defined within a certain regularization scheme at a given renormalization scale. At some low "hadronic scale" one deals with constituent (valence) degrees of freedom carrying the total hadron momentum: a constituent quark-antiquark pair in the pion case or three constituent quarks in the nucleon case [9]. The results from phenomenological studies refer to an assumed low initial scale μ_0. The value of μ_0 is not known *a priori*, but can be determined by comparing the $\langle x \rangle$-Mellin moment of pion valence PDF with $\pi - N$ DY scattering experimental data. Specifically, at $\mu = 2.0$ GeV, the valence quark is found to be $2\langle x \rangle_v = 0.47(2)$ [86,87]. At this point, under the Dokshitzer-Gribov-Lipatov-Altarelli- Parisi (DGLAP) evolution scheme of leading order (LO) we determine that μ_0 is roughly at 0.5 GeV [88], which is close to predictions based on running behavior of nonperturbative effective coupling [89,90]. In our case, the strong coupling constant is set to be the optimal value in LO global PDF analysis $\alpha_s(1.0\ \text{GeV}) = 0.68$ [91]. In the following, we shall further assume that theoretical uncertainties due to scheme dependence are smaller than the generic accuracy of LFWF approaches.

In order to compare with lattice calculation, we evolve our TMD-PDFs from $\mu^2 = \mu_0^2 = 0.25$ to $\mu^2 = 4.0\ \text{GeV}^2$. The later scale corresponds to the lattice simulation in [12]. In the parton model, the collinear unpolarized PDF is related to the unpolarized TMD-PDF as

$$f_1(x) = \int \mathrm{d}^2\mathbf{k_T} f_1(x, k_T), \quad (33)$$

which denotes the original PDF of pion and satisfies the DGLAP evolution [92–94]. The first k_T moment of the Boer-Mulders function in pion is defined as [66]

$$h_{1\pi}^{\perp(1)}(x) = \int d^2\mathbf{k_T} \frac{\mathbf{k_T}^2}{2M_\pi^2} h_{1\pi}^\perp(x, k_T), \quad (34)$$

with the pion mass $M_\pi = 130$ MeV. At the tree level, $h_{1\pi}^{\perp(1)q}(x)$ can be related to the twist-3 quark-gluon correlation function $T_{q,F}^{(\sigma)}(x, x)$ [66],

$$h_1^{\perp(1)q}(x) = \frac{1}{2M_\pi} T_{q,F}^{(\sigma)}(x, x), \quad (35)$$

whereas the QCD evolution for $T_{q,F}^{(\sigma)}(x, x)$ is given in Refs. [95,96].

For the $h_1^{\perp(1)q}(x)$ case, we follow Ref. [66] and take the evolution kernel to be [66]

$$P_{qq}^{h_1^{\perp(1)}}(x) \approx \Delta_T P_{qq}(x) - N_C \delta(1 - x), \quad (36)$$

with $\Delta_T P_{qq}(x) = C_F[\frac{2z}{(1-z)_+} + \frac{3}{2}\delta(1-x)]$. To describe the evolution of $x h_{1\pi}^{\perp(1)}(x)$, we also use the QCDNUM [88] program but insert the kernel (36) into the code. The numerical results are shown in Fig. 3. One can find that the peak of the evolved distribution shifts toward smaller x.

On the other hand, the TMD-PDFs evolution is more complicated [97,98]. Taking the unpolarized TMD-PDF as an example, it is implemented in the space Fourier conjugate to k_T,

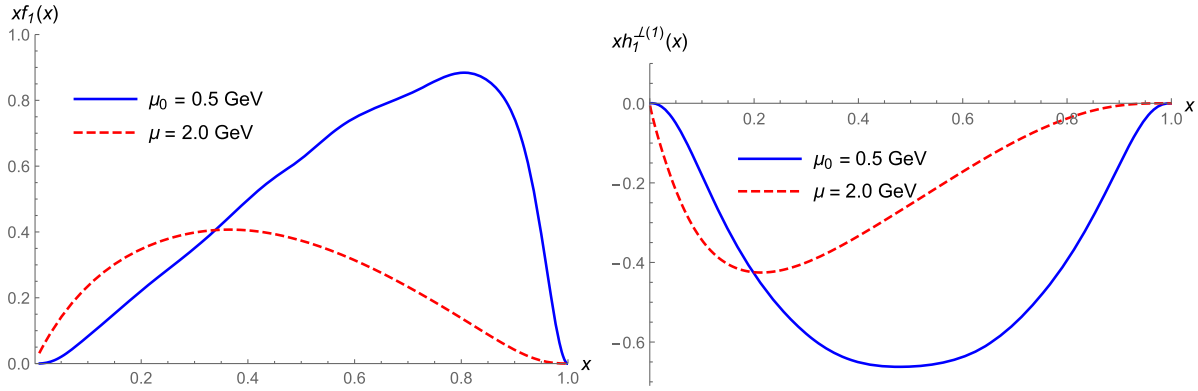

FIG. 3. Left: comparison of $xf_1(x)$ at two different scales $\mu_0 = 0.5$ GeV (blue solid) and $\mu = 2.0$ GeV (red dashed). Right: comparison of $xh_{1\pi}^{\perp(1)}(x)$ at two different scales $\mu_0 = 0.5$ GeV (blue solid) and $\mu = 2.0$ GeV (red dashed).

$$\tilde{f}_1(x, b_T^2; \mu) = \int_0^\infty dk_T k_T J_0(b_T k_T) f_1(x, k_T^2; \mu). \quad (37)$$

The TMD-PDFs generally depend on two scales, the ultraviolet renormalization scale μ and the ζ that regulates the rapidity divergence. Here, we follow the evolution prescription in [18] and set $\zeta = \mu$. The unpolarized TMD-PDF distribution in configuration space for a parton with flavor a at a certain scale μ^2 is written as [18]

$$\tilde{f}_1^a(x, b_T^2; \mu^2) = \sum_{i=q,\bar{q},g} (C_{a/i} \otimes f_1^i)(x, \bar{b}_*, \mu_b^2) \times e^{S(\mu_b^2, \mu^2)} \left(\frac{\mu^2}{\mu_b^2}\right)^{-K(\bar{b}_*;\mu_b)} \left(\frac{\mu^2}{\mu_0^2}\right)^{g_K(b_T)} \times \tilde{f}_{1\mathrm{NP}}^a(x, b_T^2). \quad (38)$$

The scale μ_b is

$$\mu_b = \frac{2e^{-\gamma_E}}{\bar{b}_*}, \quad (39)$$

where γ_E is the Euler constant and

$$\bar{b}_* \equiv \bar{b}_*(b_T; b_{\min}, b_{\max}) = b_{\max} \left(\frac{1 - e^{-b_T^4/b_{\max}^4}}{1 - e^{-b_T^4/b_{\min}^4}}\right)^{1/4}, \quad (40)$$

with

$$b_{\max} = 2e^{-\gamma_E}/\mu_0, \qquad b_{\min} = 2e^{-\gamma_E}/\mu. \quad (41)$$

The above choice guarantees that at the initial scale $\mu = \mu_0$ any effect of TMD-PDF evolution is absent. At leading order of $C_{a/i}$, the evolved TMD-PDF reduces to

$$\tilde{f}_1^a(x, b_T^2; \mu^2) = f_1^a(x; \mu_b^2) e^{S(\mu_b^2, \mu^2)} e^{\frac{1}{2} g_K(b_T) \ln(\mu^2/\mu_0^2)} \tilde{f}_{1\mathrm{NP}}^a(x, b_T^2), \quad (42)$$

where the Sudakov factor is [50]

$$S(\mu_b^2, \mu^2) = -\frac{1}{2} \int_{\mu_b^2}^{\mu^2} \frac{d\mu'^2}{\mu'^2} \left[A(\alpha_S(\mu'^2)) \ln\left(\frac{\mu^2}{\mu'^2}\right) + B(\alpha_S(\mu'^2)) \right]. \quad (43)$$

The functions A and B have perturbative expansions of the form

$$A(\alpha_S(\mu^2)) = \sum_{k=1}^{\infty} A_k \left(\frac{\alpha_S}{\pi}\right)^k, \quad B(\alpha_S(\mu^2)) = \sum_{k=1}^{\infty} B_k \left(\frac{\alpha_S}{\pi}\right)^k. \quad (44)$$

To next-to-leading logarithmic accuracy, one has [99,100]

$$A_1 = C_F, \qquad A_2 = \frac{1}{2} C_F \left[C_A \left(\frac{67}{18} - \frac{\pi^2}{6}\right) - \frac{5}{9} N_f \right], \qquad B_1 = -\frac{3}{2} C_F. \quad (45)$$

Following Refs. [101–103], the nonperturbative Sudakov factor in Eq. (42) is modeled as

$$g_K(b_T) = -g_2 b_T^2/2, \quad (46)$$

with g_2 as a free parameter. We choose $g_2 \approx 0.13$ following the findings in [18,50].

In addition to the Sudakov factors, the evolved TMD functions (42) are also related to two distribution functions, i.e., the collinear PDFs f_1^a and the intrinsic nonperturbative part of the TMD-PDF $\tilde{f}_{1\mathrm{NP}}^a$. The former can be obtained by DGLAP evolution, and the latter can be determined from the condition that Eq. (42) reduces to our calculated TMD-PDFs at initial scale, as any evolution effect should be absent at $\mu = \mu_b = \mu_0$.

The evolution of pion's Boer-Mulders function follows analogously. The Boer-Mulders function in the b_T space is defined as [104]

$$\tilde{h}^{\perp\alpha}_{1,q/\pi}(x,b_T;\mu)=\int d^2\mathbf{k_T}e^{-i\mathbf{k_T}\cdot\mathbf{b_T}}\frac{k_T^\alpha}{M_\pi}h^\perp_{1,q/\pi}(x,\mathbf{k}_T^2;\mu). \quad (47)$$

For small b_T and at leading order in α_s, it can be expressed with twist-3 correlation function [100,104,105]

$$\tilde{h}^{\alpha\perp}_{1,q/\pi}(x,b_T;\mu)=\left(\frac{-ib_T^\alpha}{2}\right)T^{(\sigma)}_{q/\pi,F}(x,x;\mu). \quad (48)$$

From Eqs. (34) and (35), one has [104]

$$T^{(\sigma)}_{q/\pi,F}(x,x;\mu)=\int d^2\mathbf{k_T}\frac{\mathbf{k_T}^2}{M_\pi}h^\perp_{1,q/\pi}(x,\mathbf{k_T}^2;\mu)=2M_\pi h^{\perp(1)}_{1,q/\pi}. \quad (49)$$

Therefore, analogous to the unpolarized TMD-PDF in Eq. (37), the evolved Boer-Mulders function of the pion in b_T space is

$$\tilde{h}^{\alpha\perp}_{1,q/\pi}(x,b_T;\mu)=\left(\frac{-ib_T^\alpha}{2}\right)e^{S(\mu_b^2,\mu^2)}e^{\frac{1}{2}g_K(b_T)\ln(\mu^2/\mu_0^2)} \times T^{(\sigma)}_{q/\pi,F}(x,x;\mu_b)\tilde{h}^{\alpha\perp}_{1,q/\pi,\mathrm{NP}}(x,b_T), \quad (50)$$

where $\tilde{h}^{\alpha\perp}_{1,q/\pi,\mathrm{NP}}(x,b_T)$ is the intrinsic nonperturbative part of the Boer-Mulders function. When $\mu=\mu_0$, the left-hand side of Eq. (50) reduces to the calculated Boer-Mulders function at initial scale.

After evolving the TMD-PDFs in b_T space, we Fourier transform the TMD-PDFs back to k_T space. In Fig. 4, we show the unpolarized TMD-PDF and Boer-Mulders function of pion evolved to the scale of $\mu=2.0$ GeV. As compared to TMD-PDFs at hadronic scale in Fig. 1, these TMD-PDFs shift toward lower x and get broader in k_T.

Finally, we compare our results with lattice calculation, focusing on a quantity named the generalized Boer-Mulders shifts [12]. For pion it has been predicted using a pion of mass $M_\pi=518$ MeV at the scale of 2 GeV [12], which is defined as

$$\langle k_T\rangle_{UT}(b_T^2;\mu^2=4.0\ \mathrm{GeV}^2) = M_\pi\frac{\tilde{h}^{\perp[1](1)}_{1,\pi}(b_T^2;\mu^2=4.0\ \mathrm{GeV}^2)}{\tilde{f}^{[1](0)}_{1,\pi}(b_T^2;\mu^2=4.0\ \mathrm{GeV}^2)}, \quad (51)$$

where the generalized TMD-PDF moments are given by

$$\tilde{f}^{[m](n)}(b_T^2)=\frac{2\pi n!}{M_\pi^{2n}}\int \mathrm{d}x x^{m-1}\int \mathrm{d}k_T k_T\left(\frac{k_T}{b_T}\right)^n \times J_n(b_Tk_T)f(x,k_T^2) \quad (52)$$

and analogously for $\tilde{h}^{\perp[1](1)}_{1,\pi}$. The lattice prediction is displayed as the data points with error bars. Our result is shown in Fig. 5 as the purple dashed line. In addition, we also include the results from the NJL model [10]. We find that, in the NJL model, the results of $M_\pi=518$ MeV is approximately 0.8 times that of 140 MeV, as indicated by both evolutions [10]. Thus, we multiply the purple curve by 0.8 and obtain the red dotted line as an estimate of pion mass variation effect. We find our results agree quite well with lattice calculation [12]. Considering the uncertainty in the nonperturbative Sudakov factor, we test with different g_2 values in Eq. (46) and find the calculated generalized Boer-Mulders shift to be insensitive to g_2. This is reasonable, as the ratio in Eq. (51) is devised to cancel the soft factors in the numerator and denominator. In Fig. 5, we also do a simple test on the influence of enforcing the positivity bound condition for TMD-PDFs at hadron scale. We modify our original Boer-Mulders function at hadron scale to be

$$\frac{k_\perp}{M_\pi}|h_1'^\perp(x,k_\perp)|)\equiv\mathrm{Max}\left[f_1(x,k_\perp),\frac{k_\perp}{M_\pi}|h_1^\perp(x,k_\perp)|)\right], \quad (53)$$

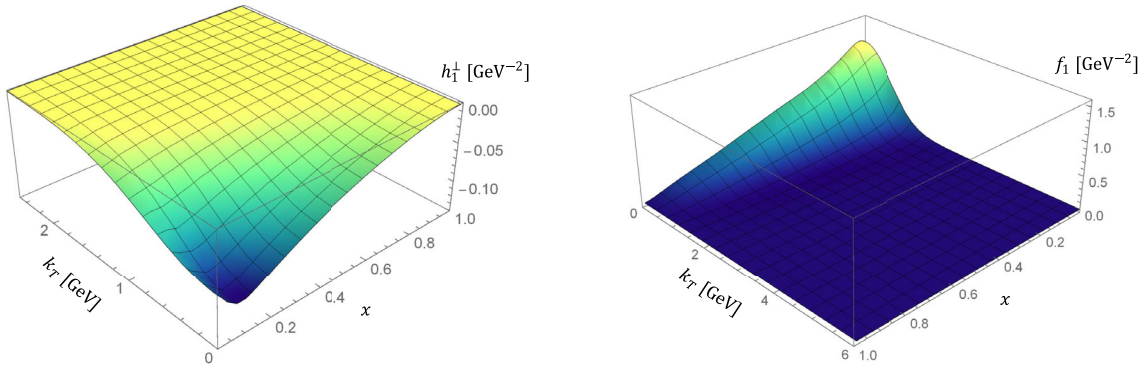

FIG. 4. Left: the evolved Boer-Mulders function generated by the nonperturbative kernel at $\mu=2.0$ GeV. Right: the evolved unpolarized TMD-PDF f_1 at $\mu=2.0$ GeV.

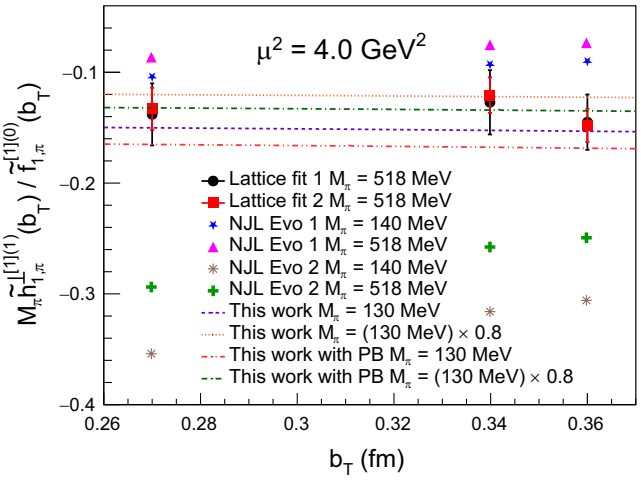

FIG. 5. The generalized Boer-Mulders shift, Eq. (51), as a function of b_T. The results of the NJL model include two types of evolution schemes, evo 1 and 2, corresponding to different evolution factors (see Ref. [10]). We indicate the generalized Boer-Mulders shift calculated using LFWFs, corresponding to pion mass $M_\pi = 130$ with the dashed line in the figure. The dotted line indicates the result of the dashed line multiplied by 0.8. Two sets of lattice data (lattice fit 1 and 2), with their rms deviation, obtained in Ref. [12] through independent fits, are shown for comparison.

where the positivity bound condition is satisfied at a minimum level. We then evolve the TMD-PDFs and find the Boer-Mulders shift decreases by 8% and remains consistent with lattice prediction.

V. CONCLUSIONS

In this work, we study the unpolarized TMD-PDF and Boer-Mulders function of pion using DS-BSEs based LFWFs. The light front overlap representation is employed. To obtain a nonvanishing Boer-Mulders function, final-state interaction analysis is utilized to construct the gluons rescattering kernel $iG(x, q_T)$, which incorporates the information of gauge link in the SU(3) case. The two leading-twist TMD-PDFs of pion at hadronic scale $\mu_0 \approx 0.5$ GeV are thus given. We then evolve both TMD-PDFs to a higher scale of 2 GeV. The generalized Boer-Mulders shift is found to be in good agreement with lattice prediction. We remark that at leading Fock state, the Boer-Mulders function is proportional to the pion's p-wave LF-LFWFs. Its emergence and magnitude is thus a reflection of the p-wave components inside pion, which essentially arises from the relativistic internal motion inside the pion. The DS-BSEs approach encapsulates such property, as well as QCD's dynamical chiral symmetry breaking property, and passes them onto the DS-BSEs based LF-LFWFs and eventually the pion TMD-PDFs.

ACKNOWLEDGMENTS

We thank Xiaoyu Wang for beneficial communications about the QCDNUM program. This work is supported by the National Natural Science Foundation of China (Grant No. 11905104) and the Strategic Priority Research Program of Chinese Academy of Sciences (Grant No. XDB34030301).

[1] D. W. Sivers, Phys. Rev. D **41**, 83 (1990).
[2] D. Boer and P. J. Mulders, Phys. Rev. D **57**, 5780 (1998).
[3] V. Barone, A. Drago, and P. G. Ratcliffe, Phys. Rep. **359**, 1 (2002).
[4] J. C. Collins, Acta Phys. Pol. B **34**, 3103 (2003), https://www.actaphys.uj.edu.pl/index_n.php?I=R7V=34&N=6#3103.
[5] R. Angeles-Martinez *et al.*, Acta Phys. Pol. B **46**, 2501 (2015).
[6] B. Pasquini, M. Pincetti, and S. Boffi, Phys. Rev. D **72**, 094029 (2005).
[7] B. Pasquini, S. Cazzaniga, and S. Boffi, Phys. Rev. D **78**, 034025 (2008).
[8] A. Bacchetta, F. Conti, and M. Radici, Phys. Rev. D **78**, 074010 (2008).
[9] B. Pasquini and P. Schweitzer, Phys. Rev. D **90**, 014050 (2014).
[10] S. Noguera and S. Scopetta, J. High Energy Phys. 11 (2015) 102.
[11] C. Shi and I. C. Cloët, Phys. Rev. Lett. **122**, 082301 (2019).
[12] M. Engelhardt, P. Hägler, B. Musch, J. Negele, and A. Schäfer, Phys. Rev. D **93**, 054501 (2016).
[13] M. A. Ebert, I. W. Stewart, and Y. Zhao, J. High Energy Phys. 09 (2019) 037.
[14] Q.-A. Zhang *et al.* (Lattice Parton Collaboration), Phys. Rev. Lett. **125**, 192001 (2020).
[15] Y. Li *et al.*, Phys. Rev. Lett. **128**, 062002 (2022).
[16] A. Bacchetta, M. Diehl, K. Goeke, A. Metz, P. J. Mulders, and M. Schlegel, J. High Energy Phys. 02 (2007) 093.
[17] X. Wang, Z. Lu, and I. Schmidt, J. High Energy Phys. 08 (2017) 137.
[18] A. Bacchetta, F. Delcarro, C. Pisano, M. Radici, and A. Signori, J. High Energy Phys. 06 (2017) 081; 06 (2019) 51.
[19] I. Scimemi and A. Vladimirov, Eur. Phys. J. C **78**, 89 (2018).
[20] A. Vladimirov, J. High Energy Phys. 10 (2019) 090.
[21] M. Bury, A. Prokudin, and A. Vladimirov, Phys. Rev. Lett. **126**, 112002 (2021).
[22] A. Bacchetta, V. Bertone, C. Bissolotti, G. Bozzi, M. Cerutti, F. Piacenza, M. Radici, and A. Signori (MAP Collaboration), J. High Energy Phys. 10 (2022) 127.

[23] M. Cerutti, L. Rossi, S. Venturini, A. Bacchetta, V. Bertone, C. Bissolotti, and M. Radici (MAP Collaboration), Phys. Rev. D **107**, 014014 (2023).
[24] J. C. Collins, Nucl. Phys. **B396**, 161 (1993).
[25] S. J. Brodsky, D. S. Hwang, and I. Schmidt, Phys. Lett. B **530**, 99 (2002).
[26] S. J. Brodsky, D. S. Hwang, and I. Schmidt, Nucl. Phys. **B642**, 344 (2002).
[27] J. C. Collins, Phys. Lett. B **536**, 43 (2002).
[28] X.-d. Ji and F. Yuan, Phys. Lett. B **543**, 66 (2002).
[29] A. V. Belitsky, X. Ji, and F. Yuan, Nucl. Phys. **B656**, 165 (2003).
[30] S. Falciano *et al.* (NA10 Collaboration), Z. Phys. C **31**, 513 (1986).
[31] M. Guanziroli *et al.* (NA10 Collaboration), Z. Phys. C **37**, 545 (1988).
[32] J. S. Conway *et al.*, Phys. Rev. D **39**, 92 (1989).
[33] F. Gautheron *et al.* (COMPASS Collaboration), Report No. SPSC-P-340, CERN-SPSC-2010-014, 2010, https://cds.cern.ch/record/1265628.
[34] M. Aghasyan *et al.* (COMPASS Collaboration), Phys. Rev. Lett. **119**, 112002 (2017).
[35] Z. Lu and B.-Q. Ma, Nucl. Phys. **A741**, 200 (2004).
[36] S. Meissner, A. Metz, M. Schlegel, and K. Goeke, J. High Energy Phys. 08 (2008) 038.
[37] X. Wang, W. Mao, and Z. Lu, Eur. Phys. J. C **78**, 643 (2018).
[38] C. Lorcé, B. Pasquini, and P. Schweitzer, Eur. Phys. J. C **76**, 415 (2016).
[39] Z. Lu, B.-Q. Ma, and J. Zhu, Phys. Rev. D **86**, 094023 (2012).
[40] F. A. Ceccopieri, A. Courtoy, S. Noguera, and S. Scopetta, Eur. Phys. J. C **78**, 644 (2018).
[41] M. Ahmady, C. Mondal, and R. Sandapen, Phys. Rev. D **100**, 054005 (2019).
[42] L. Gamberg and M. Schlegel, Phys. Lett. B **685**, 95 (2010).
[43] D. Brömmel *et al.* (QCDSF, UKQCD Collaborations), Phys. Rev. Lett. **101**, 122001 (2008).
[44] M. Diehl, T. Feldmann, R. Jakob, and P. Kroll, Nucl. Phys. **B596**, 33 (2001); **B605**, 647(E) (2001).
[45] M. Diehl, Phys. Rep. **388**, 41 (2003).
[46] C. Shi, M. Li, X. Chen, and W. Jia, Phys. Rev. D **104**, 094016 (2021).
[47] H. J. Melosh, Phys. Rev. D **9**, 1095 (1974).
[48] F. Schlumpf, Phys. Rev. D **50**, 6895 (1994).
[49] S. J. Brodsky and G. F. de Teramond, Phys. Rev. Lett. **96**, 201601 (2006).
[50] A. Bacchetta, S. Cotogno, and B. Pasquini, Phys. Lett. B **771**, 546 (2017).
[51] M. Ahmady, F. Chishtie, and R. Sandapen, Phys. Rev. D **95**, 074008 (2017).
[52] S. Jia and J. P. Vary, Phys. Rev. C **99**, 035206 (2019).
[53] Y. Li, P. Maris, and J. P. Vary, Phys. Rev. D **96**, 016022 (2017).
[54] X.-d. Ji, J.-P. Ma, and F. Yuan, Eur. Phys. J. C **33**, 75 (2004).
[55] C. Shi, K. Bednar, I. C. Cloët, and A. Freese, Phys. Rev. D **101**, 074014 (2020).
[56] C. Mezrag, H. Moutarde, and J. Rodriguez-Quintero, Few Body Syst. **57**, 729 (2016).
[57] S.-S. Xu, L. Chang, C. D. Roberts, and H.-S. Zong, Phys. Rev. D **97**, 094014 (2018).
[58] P. Maris and C. D. Roberts, Phys. Rev. C **56**, 3369 (1997).
[59] S.-x. Qin, L. Chang, Y.-x. Liu, C. D. Roberts, and D. J. Wilson, Phys. Rev. C **85**, 035202 (2012).
[60] C. Shi, Y.-P. Xie, M. Li, X. Chen, and H.-S. Zong, Phys. Rev. D **104**, L091902 (2021).
[61] C. Shi, J. Li, M. Li, X. Chen, and W. Jia, Phys. Rev. D **106**, 014026 (2022).
[62] C. Shi, J. Li, P.-L. Yin, and W. Jia, Phys. Rev. D **107**, 074009 (2023).
[63] D. Boer, Phys. Rev. D **60**, 014012 (1999).
[64] P. J. Mulders and R. D. Tangerman, Nucl. Phys. **B461**, 197 (1996); **B484**, 538(E) (1997).
[65] G. P. Lepage and S. J. Brodsky, Phys. Rev. D **22**, 2157 (1980).
[66] Z. Wang, X. Wang, and Z. Lu, Phys. Rev. D **95**, 094004 (2017).
[67] D. Boer, P. J. Mulders, and F. Pijlman, Nucl. Phys. **B667**, 201 (2003).
[68] G. R. Goldstein and L. Gamberg, in *31st International Conference on High Energy Physics* (Amsterdam, The Netherlands, 2002), pp. 452–454.
[69] D. Boer, S. J. Brodsky, and D. S. Hwang, Phys. Rev. D **67**, 054003 (2003).
[70] L. P. Gamberg, G. R. Goldstein, and K. A. Oganessyan, Phys. Rev. D **67**, 071504 (2003).
[71] L. P. Gamberg, G. R. Goldstein, and K. A. Oganessyan, Phys. Rev. D **68**, 051501 (2003).
[72] A. Bacchetta, A. Schaefer, and J.-J. Yang, Phys. Lett. B **578**, 109 (2004).
[73] Z. Lu and B.-Q. Ma, Phys. Rev. D **70**, 094044 (2004).
[74] L. P. Gamberg, G. R. Goldstein, and M. Schlegel, Phys. Rev. D **77**, 094016 (2008).
[75] M. Burkardt, Nucl. Phys. **A735**, 185 (2004).
[76] A. Bacchetta and M. Radici, Phys. Rev. Lett. **107**, 212001 (2011).
[77] B. Pasquini, S. Rodini, and A. Bacchetta, Phys. Rev. D **100**, 054039 (2019).
[78] M. Burkardt and B. Hannafious, Phys. Lett. B **658**, 130 (2008).
[79] S. Meissner, A. Metz, and M. Schlegel, J. High Energy Phys. 08 (2009) 056.
[80] C. S. Fischer and R. Alkofer, Phys. Lett. B **536**, 177 (2002).
[81] C. S. Fischer and R. Alkofer, Phys. Rev. D **67**, 094020 (2003).
[82] R. Alkofer, C. S. Fischer, F. J. Llanes-Estrada, and K. Schwenzer, Ann. Phys. (Amsterdam) **324**, 106 (2009).
[83] A. Bacchetta, M. Boglione, A. Henneman, and P. J. Mulders, Phys. Rev. Lett. **85**, 712 (2000).
[84] A. Kotzinian, in *Transversity 2008* (World Scientific, Singapore, 2009).
[85] B. Pasquini and P. Schweitzer, Phys. Rev. D **83**, 114044 (2011).
[86] P. J. Sutton, A. D. Martin, R. G. Roberts, and W. J. Stirling, Phys. Rev. D **45**, 2349 (1992).
[87] M. Gluck, E. Reya, and I. Schienbein, Eur. Phys. J. C **10**, 313 (1999).
[88] M. Botje, Comput. Phys. Commun. **182**, 490 (2011).
[89] K. Raya, Z.-F. Cui, L. Chang, J.-M. Morgado, C. D. Roberts, and J. Rodriguez-Quintero, Chin. Phys. C **46**, 013105 (2022).

[90] W. de Paula, E. Ydrefors, J. H. Nogueira Alvarenga, T. Frederico, and G. Salmè, Phys. Rev. D **105**, L071505 (2022).
[91] A. D. Martin, W. J. Stirling, R. S. Thorne, and G. Watt, Eur. Phys. J. C **63**, 189 (2009).
[92] Y. L. Dokshitzer, Sov. Phys. JETP **46**, 641 (1977), http://jetp.ras.ru/cgi-bin/e/index/e/46/4/p641?a=list.
[93] V. N. Gribov and L. N. Lipatov, Sov. J. Nucl. Phys. **15**, 438 (1972), https://cds.cern.ch/record/427157.
[94] G. Altarelli and G. Parisi, Nucl. Phys. **B126**, 298 (1977).
[95] J. Zhou, F. Yuan, and Z.-T. Liang, Phys. Rev. D **79**, 114022 (2009).
[96] Z.-B. Kang and J.-W. Qiu, Phys. Lett. B **713**, 273 (2012).
[97] J. Collins, *Foundations of Perturbative QCD* (Cambridge University Press, Cambridge, England, 2013), Vol. 32.
[98] S. M. Aybat and T. C. Rogers, Phys. Rev. D **83**, 114042 (2011).
[99] C. T. H. Davies and W. J. Stirling, Nucl. Phys. **B244**, 337 (1984).
[100] J. C. Collins, D. E. Soper, and G. F. Sterman, Nucl. Phys. **B250**, 199 (1985).
[101] P. M. Nadolsky, D. R. Stump, and C. P. Yuan, Phys. Rev. D **61**, 014003 (2000); **64**, 059903(E) (2001).
[102] F. Landry, R. Brock, P. M. Nadolsky, and C. P. Yuan, Phys. Rev. D **67**, 073016 (2003).
[103] A. V. Konychev and P. M. Nadolsky, Phys. Lett. B **633**, 710 (2006).
[104] H. Li, X. Wang, and Z. Lu, Phys. Rev. D **101**, 054013 (2020).
[105] A. Bacchetta and A. Prokudin, Nucl. Phys. **B875**, 536 (2013).